Solid-State Deuterium NMR Spectroscopy of Rhodopsin

60

Suchithranga M. D. C. Perera, Xiaolin Xu, Trivikram R. Molugu, Andrey V. Struts, and Michael F. Brown

Contents

Structural Studies of Rhodopsin Using Solid-State Deuterium NMR Spectroscopy 1253
Deuterium NMR Lineshapes 1257
Retinal Molecular Dynamics and Solid-State ^{2}H NMR Relaxation 1259
Generalized Model-Free Analysis for Nuclear Spin Relaxation Rates 1261
Retinal Dynamics in Inactive and Active Rhodopsin 1263
Challenges Ahead: Molecular Mechanism of Rhodopsin Activation 1265
References 1267

Abstract

Rhodopsin is a prototype for the large Family A of G-protein–coupled receptors (GPCRs). These proteins regulate many signaling processes, and more than 35% of human pharmaceuticals are targeted against diseases related to dysfunctions of GPCR pathways. Membrane proteins such as GPCRs are challenging to crystallize for X-ray studies. In addition, their effective molar masses in detergent solutions push the limits for solution NMR spectroscopy. By contrast, solid-state NMR allows both the structure and dynamics of membrane proteins to be

S. M. D. C. Perera · T. R. Molugu
Department of Chemistry and Biochemistry, University of Arizona, Tucson, AZ, USA

X. Xu
Department of Physics, University of Arizona, Tucson, AZ, USA

A. V. Struts
Department of Chemistry and Biochemistry, University of Arizona, Tucson, AZ, USA

Laboratory of Biomolecular NMR, St. Petersburg State University, St. Petersburg, Russia

M. F. Brown (✉)
Department of Chemistry and Biochemistry, and Department of Physics, University of Arizona, Tucson, AZ, USA
e-mail: mfbrown@u.arizona.edu

G. A. Webb (ed.), *Modern Magnetic Resonance*,
https://doi.org/10.1007/978-3-319-28388-3_144

investigated in a natural lipid bilayer environment. Here, we describe solid-state ^{2}H NMR methods for investigating structural and dynamical changes of the retinylidene cofactor of the GPCR rhodopsin upon photoillumination. Rhodopsin was regenerated with retinal containing ^{2}H-labeled C5-, C9-, or C13-methyl groups. The receptor was recombined with phospholipid membranes, which were aligned on planar glass slides. The angular dependences of the ^{2}H NMR spectra and the corresponding relaxation rates were measured for rhodopsin in the dark and in the cryo-trapped, preactive Meta-I and active Meta-II states. Analysis of the ^{2}H NMR lineshapes using a static uniaxial distribution yields orientational restraints for the retinylidene conformation when bound to the protein. Solid-state ^{2}H NMR relaxation data provide additional information on the motion of the bound cofactor. The structural and dynamical changes of retinal reveal how its functional groups (methyl groups and the β-ionone ring) affect rhodopsin light activation, and illustrate the opportunities of solid-state ^{2}H NMR spectroscopy in studying membrane proteins.

Keywords
GPCRs · Lipids · Membrane proteins · Membranes · Molecular dynamics · NMR relaxation · NMR spectroscopy · Rhodopsin activation

Membrane proteins comprise about one-third of the human genome and are responsible for regulating a variety of crucial cellular functions. Transport of proteins, small molecules, and ions across the membrane, reception of external stimuli and cellular signaling, membrane enzyme activity, and involvement in immune system function are among the crucial roles played by membrane proteins. Their location within biological membranes presents the greatest challenge limiting the techniques that can be used for studying such proteins [1]. For instance, the large size of the membrane proteins makes it difficult to use solution NMR spectroscopy; and growing high-quality membrane protein crystals as required for X-ray crystallographic studies is problematic. Advanced magnetic resonance techniques such as solid-state NMR spectroscopy thus become necessary for studying membrane proteins in a native-like lipid bilayer environment. Here, we present an application of solid-state NMR methods to membrane proteins using the visual receptor rhodopsin as the example.

Rhodopsin is the G-protein–coupled receptor responsible for the scotopic (dim light) vision of vertebrates. The chromophore 11-*cis* retinal acts as an inverse agonist, and locks the rhodopsin in the dark-state conformation. Following light absorption, it isomerizes to the all-*trans* form, releasing two ionic locks and rearranging hydrogen bonds that lead to movements of the transmembrane helices of the protein, yielding active rhodopsin. Clearly, the retinal chromophore is pivotal for maintaining the rhodopsin structure as well as its function. The temporal sequence of the photointermediates occurring during rhodopsin activation is illustrated in Fig. 1 [2, 3]. Most of these spectroscopically defined photointermediates are yet to be fully characterized, due to their transient nature, and they are trapped under various conditions such as temperature, pH, and lipid composition. The cognate G-protein of rhodopsin, transducin (G_t), is activated by the Meta-II state. The equilibrium between

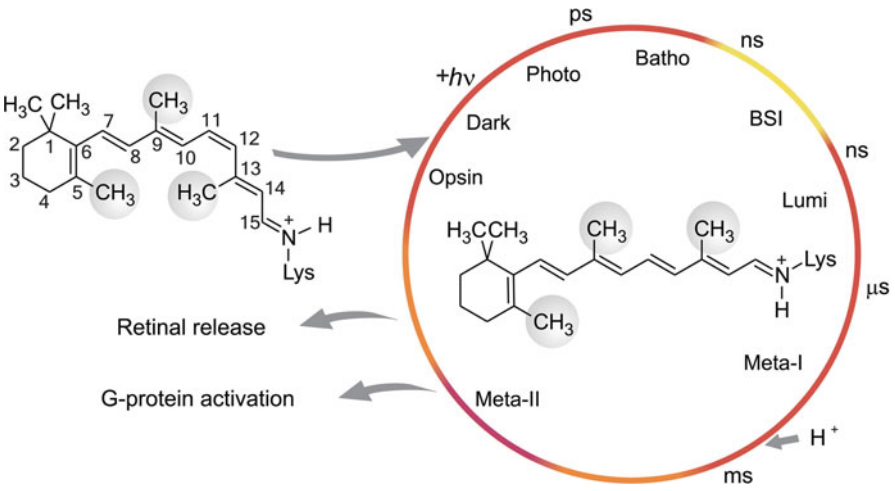

Fig. 1 Light activation of rhodopsin involves a time-ordered sequence of photointermediates. The photoillumination of rhodopsin leads to the isomerization of 11-*cis* retinal to all-*trans* retinal that in turn triggers changes in the protein structure. Activated rhodopsin occurs through a series of transient intermediates with a lifetime typically orders of magnitude greater than the preceding one. Dark-state rhodopsin goes through photorhodopsin, bathorhodopsin, blue-shifted intermediate (BSI), and lumirhodopsin, leading to equilibrium between inactive Meta-I and active Meta-II. Eventual release of all-*trans* retinal from Meta-II yields the apoprotein opsin. The active Meta-II form consists of an ensemble of states; Meta-II$_a$, Meta-II$_b$, and Meta-II$_b$H$^+$ substates as explained by an ensemble activation mechanism (Ref. [2])

the inactive Meta-I and the active Meta-II species depends on hydration, pH, and the lipid bilayer composition, allowing these metastable species to be studied by varying the above conditions. Magnetic resonance methods such as electron paramagnetic resonance (EPR) [4], solid-state ^{13}C NMR [5–12], and solid-state ^{2}H NMR spectroscopy [13–18] together with X-ray techniques [19, 20] reveal crucial information about these intermediates in the activation of rhodopsin. Here, we review the use of solid-state ^{2}H NMR spectroscopy to probe the structural and dynamical changes associated with rhodopsin activation in a natural lipid bilayer environment.

Structural Studies of Rhodopsin Using Solid-State Deuterium NMR Spectroscopy

Site-directed deuterium labeling of the retinal allows one to probe specific groups of the activating ligand. For these experiments, retinal is synthesized with ^{2}H-labeled methyl groups at positions C5, C9, or C13, namely (11-Z-[5-C^{2}H$_3$]-retinal, 11-Z-[9-C^{2}H$_3$]-retinal, or 11-Z-[13-C^{2}H$_3$]-retinal) [17]. The deuterated retinal is incorporated into the binding pocket of opsin. The regenerated rhodopsin is then recombined with synthetic phospholipids to produce a native-like environment to study the structure and dynamics of the chromophore in various states of the receptor

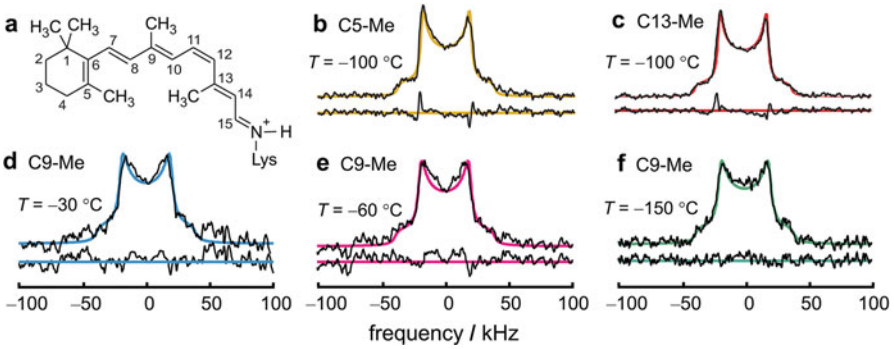

Fig. 2 Deuterium-labeled 11-*cis* retinal bound to dark-state rhodopsin in unaligned membranes yields powder-type ^{2}H NMR spectra showing rapid rotation of methyl groups. (**a**) The 11-*cis* retinal ligand with the backbone carbon atoms numbered. (**b**, **c**) Deuterium NMR spectra of ^{2}H-labeled methyl groups at C5 (*yellow*) and C13 (*red*) carbon positions, respectively, of 11-*cis* retinal in rhodopsin in unaligned POPC lipid membranes (molar ratio 1:50) at $T = -100$ °C. (**d**–**f**) Deuterium NMR spectra of ^{2}H-lableled C9-methyl group of 11-*cis* retinal bound to rhodopsin in gel-phase POPC lipid membranes at $T = -30$, -60, and -150 °C, respectively. The continuous-color lines superimposed on the experimental spectra are calculated assuming axial rotations of the methyl groups

[16–18]. Isotopic labeling of each methyl group of 11-*cis* retinal allows one to probe different regions of the binding cavity, and identify changes during the activation of rhodopsin.

The chemical structure of 11-*cis* retinal (with the carbon atoms numbered) covalently bound to Lys^{296} of helix 7 (H7) of rhodopsin is provided in Fig. 2a. Illustrative deuterium NMR spectra of rhodopsin containing retinal with deuterated methyl groups at various positions (C5, C9, and C13) in POPC lipid membranes are shown in Fig. 2b–f. Aqueous dispersions of the recombinant membranes (unaligned) yield powder-type deuterium NMR spectra, where the Pake formula, Eq. (1) as explained in Ref. [21], is used for spectral simulation:

$$|p(\xi_{\pm})| \propto \frac{1}{\left|\cos\widetilde{\theta}\right|} \propto \frac{1}{\sqrt{1 \pm 2\xi_{\pm}}} \tag{1}$$

In the above formula $p(\xi_{\pm})$ is the probability density, where $\xi_{\pm} \in [\mp\frac{1}{2}, \pm 1]$ is the reduced frequency for each of the two spectral branches, and $\widetilde{\theta}$ is the overall angle of the C–C^{2}H$_3$ bond axis to the main $\mathbf{B_0}$ magnetic field.

Use of the Pake formula and the spectral simulation provide the following information. The motion-averaged ^{2}H NMR lineshapes yield residual quadrupolar couplings (RQCs) of $\langle\chi_Q\rangle = 50.7$–$52.0$ kHz. The occurrence of rapid spinning of the retinylidene methyl groups about their threefold axes is thus established, with rotational correlation times $<10^{-5}$ s down to about -160 °C. Methyl-group order parameters of $S_{C_3} \approx 0.9$ are measured directly from the RQCs, amounting to $\approx 15°$ off-axis fluctuations. The dynamics entail methyl rotations with respect to the

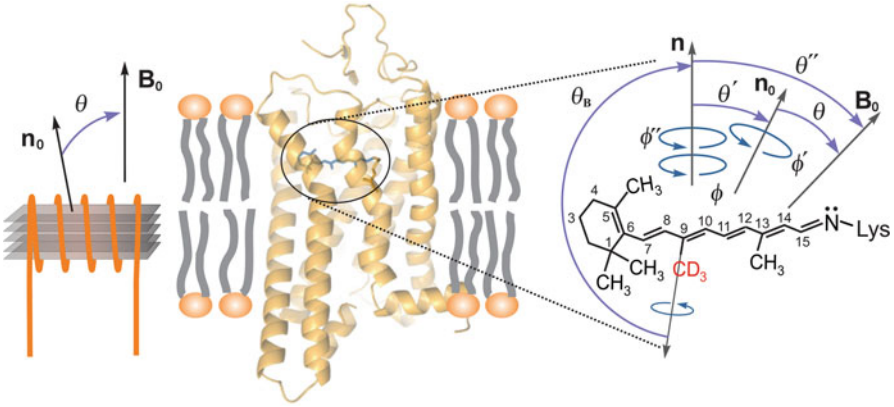

Fig. 3 Conformation and orientation of retinylidene ligand of rhodopsin are accessible by solid-state ^{2}H NMR spectroscopy of aligned membranes. *Left*: schematic depiction of stack of aligned membranes containing rhodopsin within the radiofrequency coil of the NMR spectrometer, showing the geometry relative to the magnetic field. *Center*: the seven transmembrane helices of rhodopsin are denoted by yellow ribbons, with the N-terminus above (extracellular side) and C-terminus below (cytoplasmic side). *Right*: for an individual methyl group, θ_B is angle of the C–C^{2}H$_3$ bond direction to the local bilayer normal **n**, with a static uniaxial distribution given by the azimuthal angle ϕ. The mosaic spread (alignment disorder) is described by the angle θ' of **n** to the average membrane normal $\mathbf{n_0}$, and is uniaxially distributed as given by ϕ'. The tilt angle θ is from $\mathbf{n_0}$ to the main magnetic field $\mathbf{B_0}$ about which there is cylindrical symmetry. Finally, θ'' is the angle from **n** to $\mathbf{B_0}$ where ϕ'' is the azimuthal angle. The overall angle of the C–C^{2}H$_3$ bond axis to $\mathbf{B_0}$ is denoted as $\tilde{\theta}$. Retinal is shown in the flipped all-*trans* conformation as indicative of the active Meta-II state

unsaturated polyene chain and the β-ionone ring, plus their reorientations within the binding pocket.

By aligning the POPC membranes containing rhodopsin on planar substrates, one can determine the average orientation of the C–C^{2}H$_3$ bond axis (principal axis of ^{2}H quadrupolar coupling tensor, parallel to methyl threefold axis due to fast spinning) versus the membrane normal frame. The experimental arrangement (Fig. 3) entails a stack of supported membranes including rhodopsin with retinal ^{2}H-labeled at the C5-, C9-, or C13-methyl groups. Rhodopsin is shown by the seven transmembrane helices (Fig. 3). At top right, the retinylidene ligand is depicted to illuminate the structure calculation (Fig. 3). A static uniaxial distribution is assumed, and the orientation θ_B of the C–C^{2}H$_3$ bond axis to the local membrane frame is established by calculating the ^{2}H NMR lineshape versus the tilt angle θ between the average membrane normal $\mathbf{n_0}$ and the main magnetic field $\mathbf{B_0}$ (tilt series). For aligned samples, the simulation parameters entail the C–C^{2}H$_3$ bond orientation, the residual coupling $\langle\chi_Q\rangle$, the mosaic spread σ, and the intrinsic line broadening.

Solid-state ^{2}H NMR spectra in the dark state acquired at $T = -150$ °C are shown (Fig. 4a) for aligned rhodopsin/POPC (1:50) bilayers, with retinal ^{2}H-labeled at the C5-, C9-, or C13-methyl groups, respectively. The results (Fig. 4a) were obtained for the $\theta = 0°$ orientation of the membrane normal to the magnetic field $\mathbf{B_0}$, where the

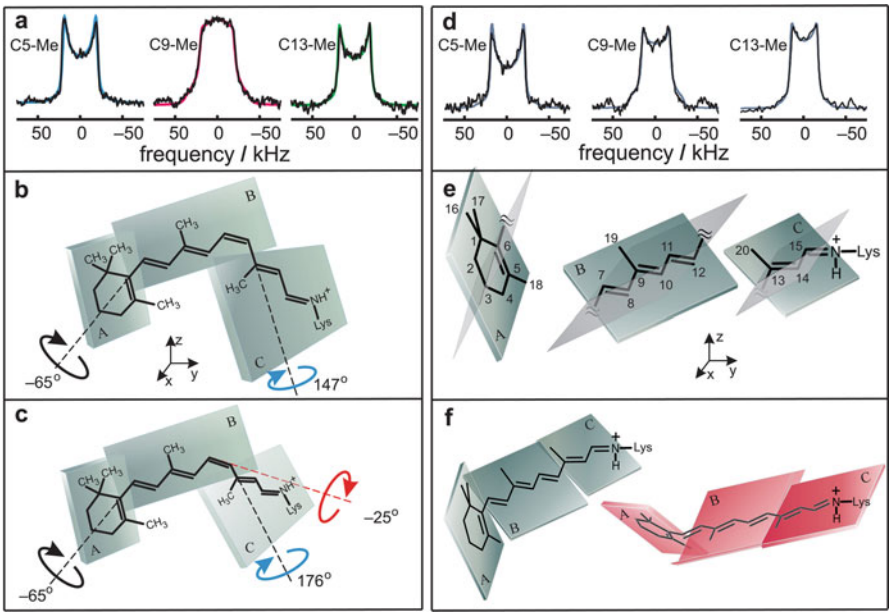

Fig. 4 Retinal structure in rhodopsin dark state and preactive Meta-I state is established by solid-state ^{2}H NMR spectroscopy. (**a**) Solid-state ^{2}H NMR spectra for 11-*cis* retinal in dark state of rhodopsin provide methyl bond orientations and disorder in aligned membranes. Examples of ^{2}H NMR spectra are shown for 11-*Z*-[5-C^{2}H$_3$]-retinylidene rhodopsin, 11-*Z*-[9-C^{2}H$_3$]-retinylidene rhodopsin, and 11-*Z*-[13-C^{2}H$_3$]-retinylidene rhodopsin, respectively. Data are included for rhodopsin/POPC bilayers (1:50) at $\theta = 0°$ alignment of membrane normal to the main magnetic field $\mathbf{B_0}$ at pH = 7 and $T = -150$ °C. (**b**) Illustration of simple three-plane model with dihedral twisting solely about C6–C7 and C12–C13 bonds. The retinal conformation is indicated by three planes of unsaturation (designated A, B, C). (**c**) Extended three-plane model with added pretwisting about C11=C12 double bond. (**d**) Solid-state ^{2}H NMR spectra are shown of retinal in preactive Meta-I state for $\theta = 0°$ orientation of membrane normal to $\mathbf{B_0}$ at pH 7 and $T = -150$ or -100 °C. (**e**) Orientations of methyl groups and electronic transition dipole moment define orientations of the planes of unsaturation; two of the four possible solutions are indicated in each case. (**f**) Examples of possible structures for retinylidene ligand with Schiff base linkage to Lys^{296} of rhodopsin. Note that different ^{2}H NMR structures for retinylidene ligand are distinguished using rotational resonance ^{13}C NMR carbon–carbon distances (see text). The extracellular side of rhodopsin is above and the cytoplasmic side below (Adapted with permission from Ref. [15])

lineshape is very sensitive to the methyl group orientation (θ_B). Similar experiments were conducted at temperatures of $T = -60$ and -30 °C. Notably, the solid-state ^{2}H NMR spectra reveal only a minor temperature variation over a broad interval of 120 °C. Theoretical simulations are overlaid on the experimental ^{2}H NMR data, and C–C^{2}H$_3$ bond orientations of 70 ± 3°, 52 ± 3°, and 68 ± 2° are found for the C5-, C9-, and C13-methyl groups of retinal in the rhodopsin dark state [16]. The data are explained by the average bond orientations and torsion angles of the retinylidene ligand bound to rhodopsin. Accurate bond orientations of the ^{2}H-labeled methyl groups are determined, despite the appreciable alignment disorder (mosaic spread

$\sigma = 18–21°$). Values for the alignment disorder are greater than in earlier studies of purple membranes containing bacteriorhodopsin [22], which may be due to rhodopsin ($M_r = 40$ kDa) being a larger molecule, together with the additional extramembranous regions [23]. These values differ from earlier work [24, 25]; yet they correspond well with X-ray studies of single rhodopsin crystals [26, 27].

Deuterium NMR Lineshapes

A simple analytical model can then be introduced (Fig. 4) for establishing the retinal conformation when bound to rhodopsin. Three planes of unsaturation are assumed, encompassing the β-ionone ring and the polyene chain to either side of the C12–C13 bond [16, 18, 28–30]. Relative orientations of the pairs of ^{2}H-labeled methyl groups are used for calculating the effective dihedral angles for the various planes of unsaturation. By conducting studies of aligned samples, the ^{2}H NMR data allow one to establish the orientation of the retinal cofactor bound to rhodopsin. Each molecular plane (here designated A, B, or C) is defined by two vectors, and thus two angular constraints are required to specify its orientation in space. The three planes have two bonds in common; hence, a total of four independent parameters (i.e., degrees of freedom) must be introduced to define the structure of the retinal molecule within its binding cavity. Because experimental data for the C1*R,S* methyl groups are currently unavailable, the electronic transition dipole moment of the retinylidene chromophore obtained from linear dichroism measurements can be used as a fourth orientational restraint [31–34].

It follows that the torsion angles $\chi_{i,k}$ between the A, B, and C planes are given by [16]:

$$\chi_{i,k} = \cos^{-1}\left(\frac{\cos\theta_i \cos\theta_B^{(i,k)} - \cos\theta_B^{(i)}}{\sin\theta_i \sin\theta_B^{(i,k)}}\right) - \cos^{-1}\left(\frac{\cos\theta_k \cos\theta_B^{(i,k)} - \cos\theta_B^{(k)}}{\sin\theta_k \sin\theta_B^{(i,k)}}\right) \quad (2)$$

In the above formula, $\theta_B^{(i)}$ and $\theta_B^{(k)}$ designate the orientations to the local membrane normal **n** of the various methyl groups within the consecutive planes. In addition, θ_i and θ_k are the angles of the two methyl axes to the C_i–C_k bond whose torsion angle is $\chi_{i,k}$ as in the case of the C6–C7 or the C12–C13 bond. Note that the C_i–C_k bond angle to the local membrane normal is $\theta_B^{(i,k)}$ and is obtained from the C9-methyl orientation, plus the transition dipole moment. For the torsion angles between the A, B, or C planes, multiple solutions are found (and multiple retinal geometries), which correspond to a single set of experimental methyl bond orientations. A total of 64 combinations for the relative orientations of the A, B, and C planes are possible for retinal bound to rhodopsin, giving 128 possible retinal configurations with the even parity taken into account (e.g., up and down orientation of the magnetic field cannot

be distinguished). What is more, circular dichroism (CD) data [29, 35] and carbon–carbon distances obtained from rotational resonance solid-state ^{13}C NMR studies [12, 36] can be introduced. It is then possible to obtain a simple physical result, in analogy to solution NMR spectroscopy.

According to these procedures, the angle between planes B and C is established using Eq. (2) to be $\chi_{9,13} = +150 \pm 4°$ ($+147 \pm 4°$) (Fig. 4b). The two values correspond to a C11=C12–C13 bond angle of 120 or 130°, respectively [15]. Note also that distortion of the C11=C12–C13 bond angle from ideal orbital geometry may take place due to steric hindrance of the C13-methyl group with the retinal hydrogen H10, or it may be induced by the rhodopsin binding pocket. Considering next the β-ionone ring, introducing positional restraints for the C8-to-C18 and C8-to-C16/C17 distances from solid-state ^{13}C NMR [36] plus the chirality known from CD studies [35], the C6–C7 dihedral angle of $\chi_{5,9} = -65 \pm 6°$ is the physical solution. It represents a negatively twisted 6-*s*-*cis* conformation (Fig. 4b). To further specify the 11-*cis*-retinylidene structure derived from solid-state ^{2}H NMR, it was inserted into the binding pocket of the rhodopsin X-ray structure (resolution of 2.2 Å; PDB accession code 1U19) [27]. The Schiff base end of retinal was superimposed with the Lys^{296} nitrogen, keeping the C12 to C15 carbon atoms near to the X-ray coordinates. Even so, a simple three-plane model did not fit into the binding pocket, because of the multiple steric clashes of retinal with the Tyr^{178} and Cys^{187} side chains of extracellular loop E2, as well as Met^{207}, Tyr^{268}, and Ala^{292} in helices H5, H6, and H7, respectively. To resolve this difficulty, an additional twist of the C11=C12 bond of the polyene chain was assumed [16, 37]. Adopting an extended three-plane model, the C11=C12 dihedral angle was established by fitting the C10-to-C20 and C11-to-C20 distances to ^{13}C NMR rotational resonance data [12]. As a result, the C11=C12 torsion angle was found to be $-25 \pm 10°$ and the C12–C13 torsion angle $176 \pm 6°$, where the twist is predominantly localized to the C11=C12 bond. Note that the C10-to-C20 and C11-to-C20 distances are less sensitive to the C11=C12 torsion angle. The structure deduced for retinal (Fig. 4c) in this way corresponds to the rhodopsin N-terminus at the top (extracellular side), and the C-terminus at the bottom (cytoplasmic side).

To summarize at this point using solid-state ^{2}H NMR spectroscopy, the structural studies reveal twisting of the retinal chromophore when bound to rhodopsin in the dark state. This finding is in accord with other biophysical studies [18, 26, 29, 30, 34, 36–45] and is key to understanding its photoreaction dynamics [46–49]. Of notable significance for rhodopsin is the torsional twisting about the C11=C12 double bond, together with the twist of the β-ionone ring [30]. The finding of a nonplanar structure of the retinal ligand is consistent with the presence of hydrogen-out-of-plane (HOOP) modes in resonance Raman [47, 49–51] and FTIR [40] spectroscopies and with circular dichroism (CD) studies [29, 38, 42, 43]. All of these features are significant to explaining how release of the photonic energy is used to initiate visual signaling by rhodopsin in the natural photoreceptor membranes [16, 29, 31, 36].

In a manner similar to the above studies, the Meta-I state can also be cryo-trapped in planar-supported bilayers to determine the changes in the retinal conformation and

orientation induced by light absorption. Solid-state ^{2}H NMR spectra acquired at -100 °C for macroscopically aligned POPC membranes at $\theta = 0°$ tilt angle allow comparison of the dark state (Fig. 4a–c) to the Meta-I state (Fig. 4d–f). For the bound retinylidene ligand, the greatest differences are found for the C9–C^{2}H$_3$ group, with smaller variations for the C5–C^{2}H$_3$ and C13–C^{2}H$_3$ groups (Fig. 4d). These differences in the ^{2}H NMR spectra manifest the bond orientation θ_B as well as the alignment disorder (mosaic spread σ). In the preactive Meta-I state, orientations are determined for the C5-, C9-, and C13-methyl groups θ_B of $72 \pm 4°$, $53 \pm 3°$, and $59 \pm 3°$, respectively. Because of the larger mosaic spread of Meta-I ($\sigma = 22$–$25°$) versus dark-state rhodopsin ($\sigma = 18$–$21°$), the ^{2}H NMR spectra for the C9-methyl differ, although the bond orientations are similar (Fig. 4d). In contrast, for the C13-methyl group, a smaller spectral difference is evident with a larger change in bond orientation. Analogous to dark-state rhodopsin, the solid-state ^{2}H NMR spectra establish that the retinylidene methyl substituents have rapid threefold rotation, with order parameters for off-axial motions of ≈0.9 within the Meta-I binding cavity (Fig. 4d).

Theoretical simulation of the solid-state ^{2}H NMR spectra [21] provides the methyl group angles, which together with the electronic transition dipole moment define the orientations of the molecular fragments. The fragments are then assembled to yield to the retinal structure when bound to the protein. Examples (two for each plane) show that multiple solutions are possible for the retinal structure (Fig. 4e). By use of Eq. (2), and including experimental rotational resonance ^{13}C NMR data [12] for the C10-to-C20 and C11-to-C20 carbon distances, the torsion angle between the B and C planes of $\chi_{9/13} = \pm 173 \pm 4°$ is found. An almost fully relaxed all-*trans* conformation occurs in the preactive Meta-I state [11, 12]. What is more, solutions for the β-ionone ring of $\chi_{5/9} = \pm 32$ and $\pm 57°$ are found as two possibilities. For the Meta-I state, the region of the polyene chain with the C13-methyl group rotates about the C11=C12 double bond toward the membrane extracellular side. Evidently, the polyene chain becomes straightened, whereby the β-ionone ring is displaced along the retinal axis toward helix H5. The calculated Meta-I structures are further restrained by placing them into the dark-state rhodopsin X-ray structure [27]. Assuming the shape of the retinal binding cavity in Meta-I resembles the dark state, most of the retinal structures were eliminated because of the different position of the β-ionone ring in the binding pocket. The exception is the retinal structure with $\chi_{5/9} = -32°$ and $\chi_{9/13} = 173°$ (left of Fig. 4f) and the structure with $\chi_{5/9} = 32°$ and $\chi_{9/13} = -173°$ obtained by reflection (mirror symmetry transformation) in a vertical plane. Even so, the first structure fits best within the binding cavity, the only close contact being with the side chain of Trp^{265}. By contrast, the mirror structure makes close contacts with the side groups of Glu^{122}, Trp^{265}, Tyr^{268}, and Ala^{292}, and thus it is less probable.

Retinal Molecular Dynamics and Solid-State ^{2}H NMR Relaxation

Turning next to the retinal dynamics, in Fig. 5 the experimental ^{2}H NMR relaxation experiments are summarized for rhodopsin in the dark state. Arrhenius-type plots of both the T_{1Z} relaxation times and T_{1Q} relaxation times are shown versus reciprocal

temperature, for those methyl groups of the bound retinal crucial to its function. One can perceive that the structural fluctuations of retinal in the dark state are unaltered by phase transitions of the lipids or by the freezing of water. The retinal cofactor is deeply buried within the receptor core (Fig. 3), and hence the relaxation data can be smoothly extrapolated to physiological temperature. For the retinylidene C5-Me group (Fig. 5a, b), a clear minimum in T_{1Z} is seen at −120 °C and for T_{1Q} at −135 °C. By contrast, for the C9- and C13-Me groups, the T_{1Z} and T_{1Q} minima occur at much lower temperatures, outside the measured range (Fig. 5c, d) [52]. According to these results, site-specific differences exist in the dynamics of the retinylidene methyl groups when bound to rhodopsin, despite that the order parameters show little variation.

As discussed above, for slower motions, the T_{1Z} and T_{1Q} minima occur at higher temperature (to the left). Conversely, for faster motions, the minima occur

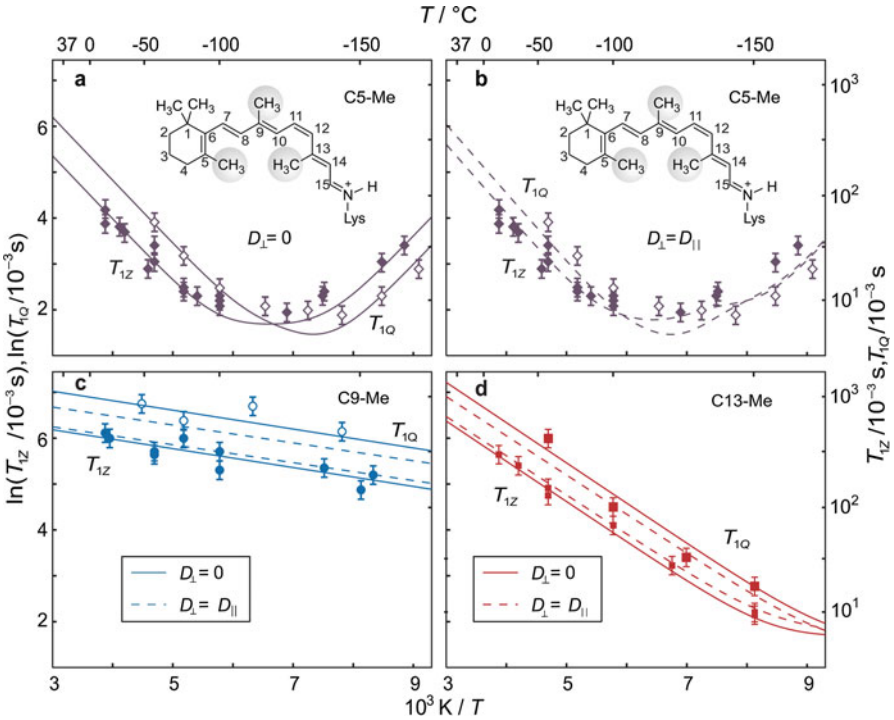

Fig. 5 Solid-state ^{2}H NMR relaxation uncovers site-specific differences in the mobility of the retinal ligand of rhodopsin. Spin-lattice (T_{1Z}) and quadrupolar-order (T_{1Q}) relaxation times are graphed against reciprocal temperature for rhodopsin in the dark state in POPC membranes (1:50 molar ratio). (**a**, **b**) Retinal ^{2}H-labeled at the C5-methyl group, (**c**) the C9-methyl group, and (**d**) the C13-methyl group. Experimental T_{1Z} and T_{1Q} times were fit using analytical models for molecular dynamics [52, 53]: axial threefold jump model (rate constant k, solid lines); and continuous rotational diffusion model (coefficients $D_\parallel$ and $D_\perp$ with solid lines for $D_\perp = 0$ and dashed lines for $D_\perp = D_\parallel$). Variations in the rates of methyl spinning are seen for the retinylidene ligand of dark-state rhodopsin in a membrane environment (Adapted with permission from Ref. [52])

at lower temperature (to the right) [13]. At a given minimum, the effective correlation time τ_c is matched to the Larmor (resonance) frequency ω_0 by $\tau_c \approx 1/\omega_0 = 13$ ns. Moreover, the correlation times are less at higher temperatures, as observed for the different retinylidene methyl groups. The comparatively short T_{1Z} and T_{1Q} relaxation times for the C5-Me group indicate a mainly 6-*s*-*cis* conformation of the β-ionone ring [18], in contrast to 6-*s*-*trans*. (For a 6-*s*-*cis* conformation, the nonbonded (1,7) interactions with hydrogen H8 would give slower spinning of the C5-Me group versus (1,6) interactions with hydrogen H7 in the 6-*s*-*trans* conformation.) What is more, the polyene C9- and C13-methyl groups have longer T_{1Z} times. They indicate greater mobility, because of the weak noncovalent interactions within the retinal ligand, and with the adjacent amino acid residues.

Generalized Model-Free Analysis for Nuclear Spin Relaxation Rates

At the initial stage, our approach [53] is evidently model free, because we directly measure the RQCs and derived C–C^{2}H$_3$ order parameters, plus the corresponding R_{1Z} relaxation rates. In the next level of analysis, the theory of nuclear spin relaxation is introduced to investigate the molecular dynamics [53]. Experimentally, the nuclear spin-lattice relaxation rates depend on thermal motions of the C–^{2}H bond (electric field gradient, EFG tensor) near the ω_0 resonance frequency, and read [53]:

$$R_{1Z} = 1/T_{1Z} = \frac{3}{4}\pi^2\chi_Q^2[J_1(\omega_0) + 4J_2(2\omega_0)] \tag{3}$$

and

$$R_{1Q} = 1/T_{1Q} = \frac{9}{4}\pi^2\chi_Q^2 J_1(\omega_0) \tag{4}$$

In the above expressions, T_{1Z} is the relaxation time for Zeeman order and T_{1Q} is that for quadrupolar order; χ_Q is the quadrupolar coupling constant; and ω_0 is the nuclear resonance (Larmor) frequency. The spectral densities of motion are denoted by $J_1(\omega_0)$ and $J_2(2\omega_0)$ and describe the power of the fluctuations at ω_0 and twice ω_0. A simple physical picture is that matching of the power spectrum of the fluctuations to the Zeeman energy level gap drives the transitions between states of different nuclear spin angular momentum [53].

The general theory of NMR relaxation [53] can then be applied to analyze in greater detail the molecular dynamics of retinal bound to rhodopsin. Generalized model-free (GMF) analysis [53] describes how the irreducible spectral densities $J_m(\omega)$ depend on the average methyl angle to the magnetic field, plus the mean-square amplitudes and rates of the motions. The spectral densities are given by:

$$J_m(\omega) = \sum_{r,q} \left|D_{0r}^{(2)}(\Omega_{\mathrm{PI}})\right|^2 \left[\left\langle \left|D_{rq}^{(2)}(\Omega_{\mathrm{IM}})\right|^2 \right\rangle - \left|\left\langle D_{rq}^{(2)}(\Omega_{\mathrm{IM}})\right\rangle\right|^2 \delta_{r0}\delta_{q0}\right] j_{rq}^{(2)}(\omega) \left|D_{qm}^{(2)}(\Omega_{\mathrm{ML}})\right|^2 \tag{5}$$

where $\omega = m\omega_0$ and $m = 1{,}2$ [54]. Here, $\mathbf{D}^{(2)}(\Omega_{ij})$ indicates the second-rank Wigner rotation matrix, and $\Omega_{ij} \equiv (\alpha_{ij}, \beta_{ij}, \gamma_{ij})$ are the Euler angles [53] for the relative orientations of the coordinate systems $\{i, j\} \equiv \{\mathrm{P, I, M, L}\}$ under consideration (see Fig. 3). In this notation P is the principal axis system for the electric field gradient tensor of the C–^{2}H bond, I specifies the instantaneous orientation of the methyl group, M the average orientation, and L the laboratory ($\mathbf{B_0}$) axis system. Notably, the mean-square amplitudes are contained in the angular brackets and denote a time-ensemble average. The corresponding reduced spectral densities are indicated by $j_{rq}^{(2)}(\omega) = 2\tau_{rq}/\left(1 + \omega^2 {\tau_{rq}}^2\right)$, where τ_{rq} are the rotational correlation times.

In the case of either membrane proteins [55] or lipids, using the GMF approach, the mean-square amplitudes are quantified by the segmental order parameters, and the rates by the motional correlation times [53]. For example, for a methyl group with Euler angles $\Omega_{\mathrm{PI}} = (0°, 70.5°, 0°)$, assuming ideal geometry, an effective coupling constant of $\chi_{\mathrm{Q}}^{\mathrm{eff}} = \chi_{\mathrm{Q}} D_{00}^{(2)}(\Omega_{\mathrm{PI}}) = -\frac{1}{3}\chi_{\mathrm{Q}}$ is obtained. The order parameter of the threefold axis describes the off-axial fluctuations, and it is defined by $S_{C_3} = \frac{1}{2}\left\langle 3\cos^2\beta_{\mathrm{IM}} - 1\right\rangle$, where β_{IM} is the angle of the methyl orientation at any instant to its average value. Further theoretical analysis entails the introduction of a motional model [53, 56] to explain the fluctuations.

Applying the above formalism to rhodopsin, the T_{1Z} times can be analyzed using either a 3-site jump model or a continuous diffusion model for rotation of the retinylidene methyl groups [53]. For N-fold jumps with a rate constant k about a single axis, the correlation times are [54, 56] $1/\tau_{rq} \rightarrow 1/\tau_r = 4k\sin^2(\pi r/N)$ leading to $1/\tau_r = 3k$ for a methyl group. Alternatively, the limit of rotational diffusion about an axis can be considered. For continuous diffusion within a potential of mean torque [57], the rotational correlation times read:

$$1/\tau_{rq} = \mu_{rq} D_\perp \Big/ \left[\left\langle \left|D_{rq}^{(2)}(\Omega_{\mathrm{IM}})\right|^2 \right\rangle - \left|\left\langle D_{rq}^{(2)}(\Omega_{\mathrm{IM}})\right\rangle\right|^2 \delta_{r0}\delta_{q0}\right] + \left(D_{||} - D_\perp\right) r^2 \tag{6}$$

Here, the symbols $D_{||}$ and $D_\perp$ indicate the axial and off-axial diffusion coefficients for methyl rotation; and the moments μ_{rq} and mean-squared moduli $\langle|D_{rq}^{(2)}(\Omega_{\mathrm{IM}})|^2\rangle$ depend on both second- and fourth-rank order parameters [57]. For a strong-collision approximation, the correlation times are those of a rigid rotor [53]: $1/\tau_{rq} \rightarrow 1/\tau_r = 6D_\perp + (D_{||} - D_\perp)r^2$. The limit of continuous diffusion, e.g., for diffusion about a single axis, $1/\tau_r = D_{||} r^2$ giving the results in Refs. [53, 56]. Finally, application of transition-state theory indicates the correlation times are inversely related to $A\ \exp(-E_a/RT)$, where A is the pre-exponential factor (k_0 or D_0) and E_a is the activation barrier (energy) for methyl rotation. For a rotational diffusion model $D_{||} = D_{0||}\ \exp(-E_{a||}/RT)$ and $D_\perp = D_{0\perp}\ \exp(-E_{a\perp}/RT)$ and analogously for a threefold jump model [13, 53, 54, 57].

Retinal Dynamics in Inactive and Active Rhodopsin

As a next step, one is able to use NMR relaxation to investigate the changes in the dynamics of the retinal ligand of rhodopsin that occur upon light absorption. Compared to the dark state, pronounced T_{1Z} differences are found in the Meta-I and Meta-II states that encapsulate the light-induced changes in the retinylidene dynamics (Fig. 6). The short T_{1Z} relaxation times measured for the C5-methyl group in the dark state (Fig. 6a) indicate the β-ionone ring has a predominantly 6-*s*-*cis* conformation [13, 37], as opposed to 6-*s*-*trans* for bacteriorhodopsin [58]. Evidently [59], the β-ionone ring retains nearly the same local environment, and is not strongly affected by transitions among the dark, Meta-I, and Meta-II states (Fig. 6b, c) [37]. A shifting of the T_{1Z} minimum for the C5-methyl to lower temperatures in Meta-II (Fig. 6c) indicates a reduction in the local correlation time, e.g., due to lowering E_a by changing the C6–C7 torsional angle and/or enhancing the ring mobility. For the functionally critical C9-Me group [60], a striking change in T_{1Z} is evident in the Meta-I and Meta-II states, due to an increase in E_a for methyl spinning within the rhodopsin-binding pocket. What is more, similar E_a barriers of the C9- and C13-methyl groups upon 11-*cis* to all-*trans* isomerization are plausible, because they are on the same side of the retinal polyene chain (Figs. 6b, c).

Application of transition state theory allows the NMR relaxation rates to be quantified in terms of the activation barriers for the motions, together with the

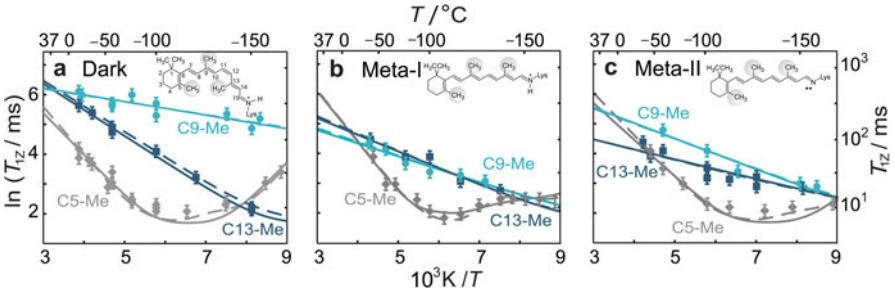

Fig. 6. Solid-state ^{2}H NMR relaxation reveals striking differences in retinal mobility during rhodopsin activation. Spin-lattice (T_{1Z}) relaxation times of retinylidene methyl groups were determined in (**a**) the dark state, (**b**) the Meta-I state, and (**c**) the active Meta-II state from $T = -30$ to -160 °C. Methyl dynamics were theoretically interpreted using an axial threefold jump model or a continuous diffusion model with coefficients $D_{\|}$ (for rotation about the C_3 axis) and $D_{\perp}$ (for off-axial reorientation). In (**a**–**c**), theoretical fits are for an axial threefold jump model or a continuous rotational diffusion model with $D_{\perp} = 0$ shown by *solid lines*. *Dashed lines* are for continuous diffusion with $D_{\perp} = D_{\|}$. In (**b**), theoretical fits for the C5-methyl group in Meta-I assume either two conformers with different bond orientations and axial diffusion coefficients (*solid line*), or one conformer with anisotropic methyl diffusion constants ($D_{\|} \neq D_{\perp}$) (*dashed line*). The results show that photoactivation of rhodopsin yields selective relaxation enhancement for C9-methyl group rotations due to nonbonded interactions of the retinal ligand with the protein (Adapted with permission from Ref. [13])

corresponding pre-exponential factors. Using transition state theory, large site-specific differences are found in the pre-exponential factors and activation barriers (E_a) (Fig. 7). For the C5-methyl substituent of the β-ionone ring (E_a = 10–15 kJ mol^{-1}), the barrier values exceed those of the other methyl groups in dark, Meta-I, and Meta-II states. For the C5-methyl group of the retinylidene ligand, the relatively high activation energy E_a (calculated from the slope of the temperature dependences of the T_{1Z} and T_{1Q} relaxation times) of ≈12 kJ mol^{-1} is usual for methyl rotations in organic solids. Steric hindrance can occur because of nonbonded, intraretinal interactions with the polyene H8 hydrogen, and/or steric clashes with amino acid residues within the binding cavity, e.g., Glu^{122} or possibly Trp^{265}. By contrast, the notably low E_a value (barrier) for the C9-methyl is most likely due to compensation of intraretinal steric interactions, as discussed below.

Quantum mechanical calculations for retinal model compounds [61, 62] confirm that the vanishingly small barrier to rotation of the C9-methyl group (E_a = 2 kJ mol^{-1} in the dark state) (Fig. 7a) is due to nonbonded (1,6) interactions with hydrogen atoms H7 and H11 of the polyene chain (see Fig. 1). In Fig. 7a, a simple explanation of why the C9-methyl group of retinal has a smaller activation energy than expected from quantum mechanical calculations for typical organic compounds is given [37, 61]. Hydrogen atoms H7 and H11 of the polyene chain have intraretinal (1,6) interactions that are approximated by a threefold rotational potential. These rotational potentials are in antiphase due to periodic eclipsing interactions; that is to say, they are offset by ≈60° giving a shallow resultant potential (Fig. 7a). Within the binding cavity, interactions with other residues are comparatively weak, because the C9-methyl is located in the space between Tyr^{268} and Thr^{118} in the crystal structure. By contrast, for the C13-methyl group near the protonated Schiff base (PSB) end of retinal (Fig. 7b), and the C5-methyl group of the β-ionone ring at the opposite end (Fig. 7c), the mobility is less because of nonbonded (1,7) interactions with hydrogens H10 and H8, respectively. For the C13-methyl group, the intermediate E_a barrier may be due to steric interactions with retinal hydrogen H10, and possibly Tyr^{268} as well.

Following light-induced isomerization of the bound retinal ligand, the most pronounced changes entail the polyene chain of retinal, rather than the β-ionone ring. In the sequence, dark to Meta-I to Meta-II, there is a systematic increase in the activation energy barrier (E_a) for the C9-methyl of the polyene chain, together with an opposite decrease for the C13-methyl substituent (Fig. 7d). For example, the activation barrier for the C9-methyl group rotation is increased about twofold; hence, its rotational dynamics become slower. Surprisingly, however, the C9-methyl group – which is essential to rhodopsin function [60] – remains as a dynamical hotspot. Following 11-*cis* to *trans* isomerization (Fig. 1), the (1,6) interactions of the C13-methyl group occur with both polyene hydrogens H11 and H15; hence, the C13-methyl barrier (E_a = 3–5 kJ mol^{-1}) becomes similar to the C9-methyl barrier in the Meta-I and Meta-II states (Fig. 7d). Perhaps most striking, the C5-methyl barrier stays almost unchanged up to the active Meta-II state (Fig. 7d), in agreement with a mainly 6-*s*-*cis* conformation of the β-ionone ring [13, 37].

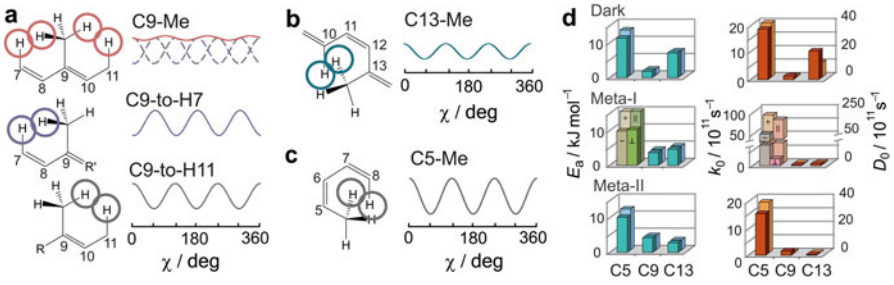

Fig. 7 Analysis of NMR relaxation data reveals site-specific dynamics of retinal underlying rhodopsin activation. The results illustrate how solid-state ^{2}H NMR relaxation probes the local energy landscape of retinal bound to rhodopsin. (**a**) Schematic methyl torsional potentials in dark state showing how the low activation barrier for C9-Me is due to antiphase (1,6) interactions with hydrogen atoms H7 and H11. (**b**, **c**) Potentials for C13- and C5-Me groups include nonbonded (1,7) interactions with hydrogen atoms H10 and H8, and reveal the energy barrier for fluctuations of the C5-methyl group is largest. (**d**) Summary of findings for the dark, Meta-I, and Meta-II states, respectively [15]. Methyl rotation is formulated as axial threefold jumps (rate constant k) or instead continuous diffusion (coefficients $D_{\|}$ and $D_{\perp}$). The pre-exponential factor is denoted by either k_0 for threefold axial jumps or D_0 for continuous diffusion; and E_a is the barrier height (activation energy). Results are shown for the diffusion model for $\eta_D \equiv D_{\|}/D_{\perp} = 1$ (in front) and $D_{\perp} = 0$ (in back). For the C5-methyl of the β-ionone ring in Meta-I, both axial ($\|$) and off-axial ($\perp$) motions are included with $\eta_D \neq 1$, or instead a two-conformer model with both positive (+) and negative (−) C5=C6–C7=C8 dihedral angles and $D_{\perp} = 0$. Note that local roughness of the potential energy landscape corresponds to site-specific variations in barriers for methyl spinning of the retinylidene ligand of rhodopsin (Adapted with permission from Refs. [15, 37])

Challenges Ahead: Molecular Mechanism of Rhodopsin Activation

Obviously, many important details of the activation mechanism of rhodopsin in a natural membrane environment remain unsolved. Because the secondary and tertiary structures of the *Rhodopsin* (Family A) GPCRs are similar, the local interactions are expected to be crucially important for targeted drug design. For rhodopsin, despite that several X-ray crystal structures including Meta-II-like structures are available, the orientation of the chromophore is still uncertain. What is more, there is a controversy between X-ray and solid-state ^{13}C NMR results. Notably, the retinal conformation in the active Meta-II state needs to be established with a high degree of certainty [63, 64]. The molecular dynamics of the retinal ligand and the rhodopsin overall structure in the activation mechanism are very important in the receptor activation, and probably other GPCRs as well. For studying GPCRs, a combination of different techniques is salutary, including molecular simulation methods that connect snapshots provided by X-ray and NMR studies of rhodopsin [52, 64], both in crystals as well as a natural lipid membrane environment.

Our current understanding of rhodopsin activation by retinal [13, 37] (Fig. 8) allows us to propose how local (ps–ns) motions of the ligand initiate the large-scale (ms) functional protein motions (Fig. 8a) [65–67]. In the inactive dark state, the low

energy barrier to rotations of the C9-methyl group signifies a lack of steric clashes, because it occupies a slot between Tyr^{268} and Thr^{118}. The C9-methyl group acts effectively as a hinge point for retinal isomerization, causing the C13-methyl and the $C{=}NH^{+}$ groups to change their positions upon light activation (Fig. 8a). In the Meta-I NMR structure of retinal [13, 15, 16, 37], rotation of the C13-methyl shifts the β_4 strand of the E2 loop upward to the extracellular (*e*) side (Fig. 8b). A hydrogen-bonding network involving TM helices H4–H6 is disrupted, as implied by a decrease in the rotational barrier (E_a) for the C13-methyl group. At the other end of the retinal ligand, the β-ionone ring is shifted toward the helix H5. A closer packing for the C5-methyl is suggested by the comparatively high E_a value in the Meta-I state (Fig. 7d). The first ionic lock of the retinylidene PSB on helix H7 with its complex counterion due to Glu^{113} (H3) and Glu^{181} (E2) is broken by internal proton transfer from the PSB to Glu^{113} in Meta-II. Elongation of retinal displaces the β-ionone ring away from Trp^{265} (H6) toward the H5–H6 helical interface [37, 63]. Initial tilting of helix H6 away from the H1–H4 helical core is accompanied by restructuring of helix H5, bringing Tyr^{223} closer to Arg^{135} and Gly^{231} near to Glu^{247} (Fig. 8c) [66]. This destabilizes the second ionic lock involving Glu^{134} and Arg^{135} of the conserved E(D)RY sequence of helix H3 plus Glu^{247} of helix H6 [66], transiently exposing the recognition sites for transducin (G_t) on the cytoplasmic face (*c*-side) (Fig. 8c) [67]. In the above model, rhodopsin activation entails collective movements of transmembrane helices H5 and H6, together with the cytoplasmic loops in the Meta-I to Meta-II equilibrium. The reversible helix fluctuations [65, 67] happen at kHz frequencies, matching the catalytic turnover rate for G_t binding and activation by rhodopsin [68]. Receptor activation thus entails a fluctuating equilibrium among states and substates on the energy landscape [13, 37]. A key question for future research is

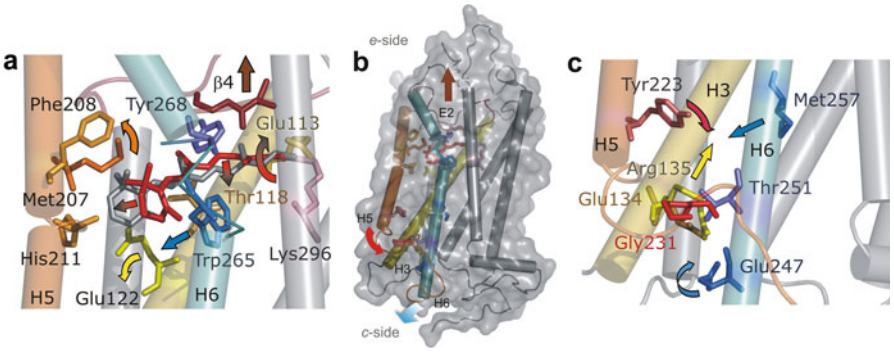

Fig. 8. Proposed activation mechanism for rhodopsin in membranes based on solid-state NMR [13] and X-ray [19] data. The extracellular side of rhodopsin is above and the cytoplasmic side below. (**a**) Isomerization of retinal (*red*) displaces the extracellular E2 loop toward the membrane surface (*e*-side). (**b**) Elongation of transmembrane helix H5 and tilting of helix H6 away from the H1–H4 helical core opens a binding cleft for the G-protein transducin. (**c**) Fluctuations of transmembrane helices H5 and H6 of rhodopsin occur in conjunction with exposing recognition sites on the opposing cytoplasmic membrane surface (*c*-side) for transducin (G_t) in the catalytic activation mechanism (Adapted with permission from Ref. [13])

whether one can quantitatively trap a single activated rhodopsin species, or whether the receptor activation requires the dynamics of a conformational ensemble unlocked by photoisomerization of the retinal ligand.

References

1. Perera SMDC, Chawla U, Brown MF. Powdered G-protein-coupled receptors. J Phys Chem Lett. 2016;7:4230–5.
2. Mertz B, Struts AV, Feller SE, Brown MF. Molecular simulations and solid-state NMR investigate dynamical structure in rhodopsin activation. Biochim Biophys Acta. 2012;1818:241–51.
3. Jäger S, Szundi I, Lewis JW, Mah TL, Kliger DS. Effects of pH on rhodopsin photointermediates from lumirhodopsin to metarhodopsin II. Biochemistry. 1998;37:6998–7005.
4. Altenbach C, Kusnetzow AK, Ernst OP, Hofmann KP, Hubbell WL. High-resolution distance mapping in rhodopsin reveals the pattern of helix movement due to activation. Proc Natl Acad Sci USA. 2008;105:7439–44.
5. Ahuja S, Eilers M, Hirshfeld A, Yan ECY, Ziliox M, Sakmar TP, Sheves M, Smith SO. 6-*s*-*cis* conformation and polar binding pocket of the retinal chromophore in the photoactivated state of rhodopsin. J Am Chem Soc. 2009;131:15160–9.
6. Ahuja S, Hornak V, Yan ECY, Syrett N, Goncalves JA, Hirshfeld A, Ziliox M, Sakmar TP, Sheves M, Reeves PJ, Smith SO, Eilers M. Helix movement is coupled to displacement of the second extracellular loop in rhodopsin activation. Nat Struct Mol Biol. 2009;16:168–75.
7. Ahuja S, Crocker E, Eilers M, Hornak V, Hirshfeld A, Ziliox M, Syrett N, Reeves PJ, Khorana HG, Sheves M, Smith SO. Location of the retinal chromophore in the activated state of rhodopsin. J Biol Chem. 2009;284:10190–201.
8. Crocker E, Eilers M, Ahuja S, Hornak V, Hirshfeld A, Sheves M, Smith SO. Location of Trp265 in metarhodopsin II: implications for the activation mechanism of the visual receptor rhodopsin. J Mol Biol. 2006;357:163–72.
9. Eilers M, Reeves PJ, Ying W, Khorana HG, Smith SO. Magic angle spinning NMR of the protonated retinylidene Schiff base nitrogen in rhodopsin: expression of ^{15}N-lysine- and ^{13}C-glycine-labeled opsin in a stable cell line. Proc Natl Acad Sci USA. 1999;96:487–92.
10. Creemers AFL, Kiihne S, Bovee-Geurts PHM, DeGrip WJ, Lugtenburg J, de Groot HJM. ^{1}H and ^{13}C MAS NMR evidence for pronounced ligand-protein interactions involving the ionone ring of the retinylidene chromophore in rhodopsin. Proc Natl Acad Sci USA. 2002;99:9101–6.
11. Feng X, Verdegem PJE, Edén M, Sandström D, Lee YK, Bovee-Geurts PHM, de Grip WJ, Lugtenburg J, de Groot HJM, Levitt MH. Determination of a molecular torsional angle in the metarhodopsin-I photointermediate of rhodopsin by double-quantum solid-state NMR. J Biomol NMR. 2000;16:1–8.
12. Verdegem PJE, Bovee-Geurts PHM, de Grip WJ, Lugtenburg J, de Groot HJM. Retinylidene ligand structure in bovine rhodopsin, metarhodopsin-I, and 10-methylrhodopsin from internuclear distance measurements using ^{13}C-labeling and 1-D rotational resonance MAS NMR. Biochemistry. 1999;38:11316–24.
13. Struts AV, Salgado GFJ, Martínez-Mayorga K, Brown MF. Retinal dynamics underlie its switch from inverse agonist to agonist during rhodopsin activation. Nat Struct Mol Biol. 2011;18:392–4.
14. Smith SO. Structure and activation of the visual pigment rhodopsin. Annu Rev Biophys. 2010;39:309–28.
15. Brown MF, Salgado GFJ, Struts AV. Retinal dynamics during light activation of rhodopsin revealed by solid-state NMR spectroscopy. Biochim Biophys Acta. 2010;1798:177–93.
16. Struts AV, Salgado GFJ, Tanaka K, Krane S, Nakanishi K, Brown MF. Structural analysis and dynamics of retinal chromophore in dark and Meta I states of rhodopsin from ^{2}H NMR of aligned membranes. J Mol Biol. 2007;372:50–66.

17. Salgado GFJ, Struts AV, Tanaka K, Krane S, Nakanishi K, Brown MF. Solid-state ^{2}H NMR structure of retinal in metarhodopsin I. J Am Chem Soc. 2006;128:11067–71.
18. Salgado GFJ, Struts AV, Tanaka K, Fujioka N, Nakanishi K, Brown MF. Deuterium NMR structure of retinal in the ground state of rhodopsin. Biochemistry. 2004;43:12819–28.
19. Standfuss J, Edwards PC, D'Antona A, Fransen M, Xie G, Oprian DD, Schertler GFX. The structural basis of agonist-induced activation in constitutively active rhodopsin. Nature. 2011;471:656–60.
20. Malmerberg E, Bovee-Geurts PHM, Katona G, Deupi X, Arnlund D, Wickstrand C, Johansson LC, Westenhoff S, Nazarenko E, Schertler GFX, Menzel A, de Grip WJ, Neutze R. Conformational activation of visual rhodopsin in native disc membranes. Sci Signal. 2015;8:ra26.
21. Nevzorov AA, Moltke S, Heyn MP, Brown MF. Solid-state NMR line shapes of uniaxially oriented immobile systems. J Am Chem Soc. 1999;121:7636–43.
22. Moltke S, Nevzorov AA, Sakai N, Wallat I, Job C, Nakanishi K, Heyn MP, Brown MF. Chromophore orientation in bacteriorhodopsin determined from the angular dependence of deuterium NMR spectra of oriented purple membranes. Biochemistry. 1998;37:11821–35.
23. Huber T, Botelho AV, Beyer K, Brown MF. Membrane model for the GPCR prototype rhodopsin: hydrophobic interface and dynamical structure. Biophys J. 2004;86:2078–100.
24. Gröbner G, Choi G, Burnett IJ, Glaubitz C, Verdegem PJE, Lugtenberg J, Watts A. Photoreceptor rhodopsin: structural and conformational study of its chromophore 11-*cis* retinal in oriented membranes by deuterium solid state NMR. FEBS Lett. 1998;422:201–4.
25. Gröbner G, Burnett IJ, Glaubitz C, Choi G, Mason AJ, Watts A. Observations of light-induced structural changes of retinal within rhodopsin. Nature. 2000;405:810–3.
26. Teller DC, Okada T, Behnke CA, Palczewski K, Stenkamp RE. Advances in determination of a high-resolution three-dimensional structure of rhodopsin, a model of G-protein-coupled receptors (GPCRs). Biochemistry. 2001;40:7761–72.
27. Okada T, Sugihara M, Bondar A-N, Elstner M, Entel P, Buss V. The retinal conformation and its environment in rhodopsin in light of a new 2.2 Å crystal structure. J Mol Biol. 2004;342:571–83.
28. Nakanishi K, Crouch R. Application of artificial pigments to structure determination and study of photoinduced transformations of retinal proteins. Isr J Chem. 1995;35:253–72.
29. Fujimoto Y, Fishkin N, Pescitelli G, Decatur J, Berova N, Nakanishi K. Solution and biologically relevant conformations of enantiomeric 11-*cis*-locked cyclopropyl retinals. J Am Chem Soc. 2002;124:7294–302.
30. Fishkin N, Berova N, Nakanishi K. Primary events in dim light vision: a chemical and spectroscopic approach toward understanding protein/chromophore interactions in rhodopsin. Chem Rec. 2004;4:120–35.
31. Chabre M, Breton J. The orientation of the chromophore of vertebrate rhodopsin in the "meta" intermediate states and the reversibility of the meta II-meta III transition. Vis Res. 1979;19:1005–18.
32. Michel-Villaz M, Roche C, Chabre M. Orientational changes of the absorbing dipole of retinal upon the conversion of rhodopsin to bathorhodopsin, lumirhodopsin, and isorhodopsin. Biophys J. 1982;37:603–16.
33. Lewis JW, Einterz CM, Hug SJ, Kliger DS. Transition dipole orientations in the early photolysis intermediates of rhodopsin. Biophys J. 1989;56:1101–11.
34. Jäger S, Lewis JW, Zvyaga TA, Szundi I, Sakmar TP, Kliger DS. Chromophore structural changes in rhodopsin from nanoseconds to microseconds following pigment photolysis. Proc Natl Acad Sci USA. 1997;94:8557–62.
35. Fujimoto Y, Ishihara J, Maki S, Fujioka N, Wang T, Furuta T, Fishkin N, Borhan B, Berova N, Nakanishi K. On the bioactive conformation of the rhodopsin chromophore: absolute sense of twist around the 6-*s*-*cis* bond. Chem Eur J. 2001;7:4198–204.

36. Spooner PJR, Sharples JM, Verhoeven MA, Lugtenberg J, Glaubitz C, Watts A. Relative orientation between the β-ionone ring and the polyene chain for the chromophore of rhodopsin in native membranes. Biochemistry. 2002;41:7549–55.
37. Struts AV, Salgado GFJ, Brown MF. Solid-state ^{2}H NMR relaxation illuminates functional dynamics of retinal cofactor in membrane activation of rhodopsin. Proc Natl Acad Sci USA. 2011;108;8263–8.
38. Yoshizawa T, Shichida Y. Low-temperature circular dichroism of intermediates of rhodopsin. Methods Enzymol. 1982;81:634–41.
39. Smith SO, Palings I, Copié V, Raleigh DP, Courtin J, Pardoen JA, Lugtenberg J, Mathies RA, Griffin RG. Low-temperature solid-state ^{13}C NMR studies of the retinal chromophore in rhodopsin. Biochemistry. 1987;26:1606–11.
40. Siebert F. Application of FTIR spectroscopy to the investigation of dark structures and photoreactions of visual pigments. Isr J Chem. 1995;35:309–23.
41. Imamoto Y, Sakai M, Katsuta Y, Wada A, Ito M, Shichida Y. Structure around C_6–C_7 bond of the chromphore in bathorhodopsin: low-temperature spectroscopy of 6s-*cis*-locked bicyclic rhodopsin analogs. Biochemistry. 1996;35:6257–62.
42. Kochendoerfer GG, Verdegem PJE, van der Hoef I, Lugtenburg J, Mathies RA. Retinal analog study of the role of steric interactions in the excited state isomerization dynamics of rhodopsin. Biochemistry. 1996;35:16230–40.
43. DeLange F, Bovee-Geurts PHM, VanOostrum J, Portier MD, Verdegem PJE, Lugtenburg J, DeGrip WJ. An additional methyl group at the 10-position of retinal dramatically slows down the kinetics of the rhodopsin photocascade. Biochemistry. 1998;37:1411–20.
44. Gascon JA, Batista VS. QM/MM study of energy storage and molecular rearrangments due to the primary event in vision. Biophys J. 2004;87:2931–41.
45. Sugihara M, Hufen J, Buss V. Origin and consequences of steric strain in the rhodopsin binding pocket. Biochemistry. 2006;45:801–10.
46. Wang Q, Schoenlein RW, Peteanu LA, Mathies RA, Shank CV. Vibrationally coherent photochemistry in the femtosecond primary event of vision. Science. 1994;266:422–4.
47. Lin SW, Groesbeek M, van der Hoef I, Verdegem P, Lugtenburg J, Mathies RA. Vibrational assignment of torsional normal modes of rhodopsin: probing excited-state isomerization dynamics along the reactive C_{11}=C_{12} torsion coordinate. J Phys Chem B. 1998;102:2787–806.
48. Andruniów T, Ferré N, Olivucci M. Structure, initial excited-state relaxation, and energy storage of rhodopsin resolved at the multiconfigurational perturbation theory level. Proc Natl Acad Sci USA. 2004;101:17908–13.
49. Kukura P, McCamant DW, Yoon S, Wandschneider DB, Mathies RA. Structural observation of the primary isomerization in vision with femtosecond-stimulated Raman. Science. 2005;310:1006–9.
50. Pan D, Mathies RA. Chromophore structure in lumirhodopsin and metarhodopsin I by time-resolved resonance Raman microchip spectroscopy. Biochemistry. 2001;40:7929–36.
51. Yan ECY, Kazmi MA, Ganim Z, Hou J-M, Pan D, Chang BSW, Sakmar TP, Mathies RA. Retinal counterion switch in the photoactivation of the G protein-coupled receptor rhodopsin. Proc Natl Acad Sci USA. 2003;100:9262–7.
52. Brown MF, Struts AV. Structural dynamics of retinal in rhodopsin activation viewed by solid-state ^{2}H NMR spectroscopy. In: Separovic F, Naito A (eds) Advances in Biological Solid-State NMR: Proteins and Membrane-Active Peptides. Cambridge, R Soc Chem. 2014;320–52.
53. Brown MF. Theory of spin-lattice relaxation in lipid bilayers and biological membranes. ^{2}H and ^{14}N quadrupolar relaxation. J Chem Phys. 1982;77:1576–99.
54. Nevzorov AA, Trouard TP, Brown MF. Lipid bilayer dynamics from simultaneous analysis of orientation and frequency dependence of deuterium spin-lattice and quadrupolar order relaxation. Phys Rev E. 1998;58:2259–81.
55. McDermott A. Structure and dynamics of membrane proteins by magic angle spinning solid-state NMR. Annu Rev Biophys. 2009;38:385–403.
56. Torchia DA, Szabo A. Spin-lattice relaxation in solids. J Magn Reson. 1982;49:107–21.

57. Trouard TP, Alam TM, Brown MF. Angular dependence of deuterium spin-lattice relaxation rates of macroscopically oriented dilaurylphosphatidylcholine in the liquid-crystalline state. J Chem Phys. 1994;101:5229–61.
58. Copié V, McDermott AE, Beshah K, Williams JC, Spyker-Assink M, Gebhard RT, Lugtenberg J, Herzfeld J, Griffin RG. Deuterium solid-state NMR studies of methyl group dynamics in bacteriorhodopsin and retinal model compounds: evidence for a 6-s-trans chromophore in the protein. Biochemistry. 1994;33:3280–6.
59. Borhan B, Souto ML, Imai H, Shichida Y, Nakanishi K. Movement of retinal along the visual transduction path. Science. 2000;288:2209–12.
60. Vogel R, Lüdeke S, Siebert F, Sakmar TP, Hirshfeld A, Sheves M. Agonists and partial agonists of rhodopsin: retinal polyene methylation affects receptor activation. Biochemistry. 2006;45:1640–52.
61. Mertz B, Lu M, Brown MF, Feller SE. Steric and electronic influences on the torsional energy landscape of retinal. Biophys J. 2011;101:L17–9.
62. Zhu S, Brown MF, Feller SE. Retinal conformation governs pK_a of protonated Schiff base in rhodopsin activation. J Am Chem Soc. 2013;135:9391–8.
63. Struts AV, Xu X, Molugu TR, Pitman MC, Faylough S, Guruge C, Nascimento CL, Nesnas N, Brown MF. Activation of GPCR rhodopsin investigated by solid-state NMR spectroscopy. Biophys J. 2017;112:508a.
64. Kimata N, Pope A, Eilers M, Opefi CA, Ziliox M, Hirshfeld A, Zaitseva E, Vogel R, Sheves M, Reeves PJ, Smith SO. Retinal orientation and interactions in rhodopsin reveal a two-stage trigger mechanism for activation. Nat Commun. 2016;7:12683.
65. Knierim B, Hofmann KP, Ernst OP, Hubbell WL. Sequence of late molecular events in the activation of rhodopsin. Proc Natl Acad Sci USA. 2007;104:20290–5.
66. Park JH, Scheerer P, Hofmann KP, Choe H-W, Ernst OP. Crystal structure of the ligand-free G-protein-coupled receptor opsin. Nature. 2008;454:183–8.
67. Mahalingam M, Martínez-Mayorga K, Brown MF, Vogel R. Two protonation switches control rhodopsin activation in membranes. Proc Natl Acad Sci USA. 2008;105:17795–800.
68. Ernst OP, Gramse V, Kolbe M, Hofmann KP, Heck M. Monomeric G protein-coupled receptor rhodopsin in solution activates its G protein transducin at the diffusion limit. Proc Natl Acad Sci USA. 2007;104:10859–64.